Lawrence Berkeley Laboratory
UNIVERSITY OF CALIFORNIA



Presented at the International Conference on
Nucleus-Nucleus Collisions, Michigan State University,
East Lansing, MI, September 26-October 1, 1982;
and the Detector Workshop in Memory of Hans Geiger,
Berlin, West Germany, October 6-8, 1982

# 4π PHYSICS WITH THE PLASTIC BALL

H.H. Gutbrod, H. Löhner, A.M. Poskanzer, T. Renner,
H. Riedesel, H.G. Ritter, A. Warwick, F. Weik,
and H. Wieman

October 1982



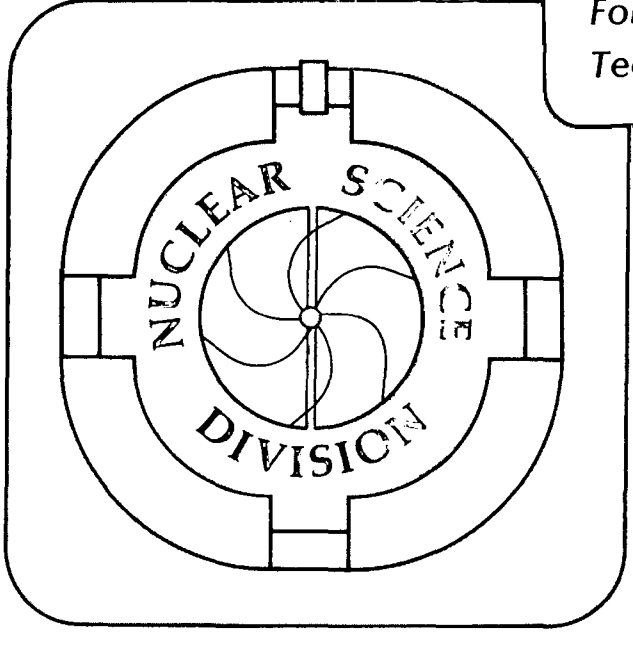


Prepared for the U.S. Department of Energy under Contract DE-AC03-76SF00098

## DISCLAIMER

LBL-14980

# $4\pi$ PHYSICS WITH THE PLASTIC BALL

H.H. GUTBROD, H. LÖHNER, A.M. POSKANZER, T. RENNER,
H. RIEDESEL, H.G. RITTER, A. WARWICK, F. WEIK, H. WIEMAN

Gesellschaft für Schwerionenforschung, Planckstrasse 1
D-6300 Darmstadt 11, West Germany

and

Nuclear Science Division, Lawrence Berkeley Laboratory
University of California, Berkeley, CA 94720

Presented at the International Conference on Nucleus-Nucleus Collisions, Michigan State University, September 26-October 1, 1982
and at the Detector Workshop in Memory of Hans Geiger, Berlin, West Germany, October 6-8, 1982

This work was supported in part by the Director, Office of Energy Research, Division of Nuclear Physics of the Office of High Energy and Nuclear Physics of the U.S. Department of Energy under Contract DE-AC03-76SF00098.

# $4\pi$ PHYSICS WITH THE PLASTIC BALL

H.H. GUTBROD, H. LÖHNER, A.M. POSKANZER, T. RENNER,
H. RIEDESEL, H.G. RITTER, A. WARWICK, F. WEIK, H. WIEMAN

Gesellschaft für Schwerionenforschung, Planckstrasse 1
D-6300 Darmstadt 11, West Germany
and
Nuclear Science Division, Lawrence Berkeley Laboratory
University of California, Berkeley, CA 94720

Abstract:
$4\pi$ data taken with the Plastic Ball show that cluster production in relativistic nuclear collisions depends on both the size of the participant volume and the finite size of the cluster. The measurement of the degree of thermalization and the search for collective flow will permit the study of the applicability of macroscopic concepts such as temperature and density.

## 1. Introduction

After several years of studying relativistic nuclear collisions one of the main goals still is to learn about the equation of state or even to find extreme states of nuclear matter. Most of the time past was used to get oriented and to learn about the environment of problem areas and about the phase space of these reactions. At energies of few hundred MeV/nucleon to 2 GeV/nucleon one soon realized that no pool but a tiny one of proton-nucleus data exists where one could dwell on for comparison with nucleus-nucleus collisions.

With their huge number of exit channels the nuclear collisions viewed by single particle detection schemes looked "thermal" in all channels. Early multi-particle detection schemes paved the way to nowadays $4\pi$ detectors that reflect our respect for the complexity of relativistic nuclear collisions.

The design criteria for the Plastic Ball were to measure so much of an event that dynamics in the event could be separated from the background of phase space population. Large dynamical effects are predicted on the one side by hydrodynamic models whereas on the other the nuclear fireball model totally ignores them. So the measurement of particles over a wide energy range under all angles is needed for coping with the observed large multiplicities of more than 100 particles.

Since we are looking for matter properties and since large cluster production has been observed in earlier experiments a good particle identification was mandatory of a $4\pi$ detector for nuclear collisions. Positive pion data had focused the attention onto their production mechanism. Therefore a $4\pi$ detector had to allow to observe the pion channels as well. At the time of conception of the Plastic Ball design one could summarize those goals by only one:

"Measure as much of the event as possible."

During the construction period and provoked by streamer chamber results, the global analysis concept for $4\pi$ data was introduced into this field from particle physics, and clear differences between intranuclear cascade calculations and hydrodynamical model calculations did show up due to a collective flow predicted by the latter model.

Before the $4\pi$ physics is discussed on the first experiments an extensive report on the Plastic Ball is given to familiarize the reader with the details of this first electronic $4\pi$ detector with particle identification capability.

A concept of a $4\pi$ detector consisting of many individual $\Delta E$-E and time-of-flight telescopes was chosen that promises fast data analysis. The number of counters necessary to cover $4\pi$ is related strongly to the multiplicities of the events to be studied, since too few large counters would result in a high probability of multiple firing. Too many small counters for a given size of the $4\pi$ detector volume, however, would cause a large percentage of the particles to scatter out of the detectors into neighboring ones.

For the coverage of most of $4\pi$ the Plastic Ball was built, completely surrounding the target except for the very backward angles where the beam enters the system and the extreme forward angles. These forward angles of $0^\circ$-$9^\circ$ are covered with a multielement time-of-flight system (called the Plastic Wall) taking into account the large fragment velocities at forward angles. The following gives a detailed description of the whole system, as it is schematically shown in Fig. 1.

## 2.1 GEOMETRY

The geometry of the Plastic Ball was selected with specific consideration of earlier multiplicity distribution measurements[1]). Since the $4\pi$ detector is to be used at various incident energies, its spatial resolution, and thus the number and dimensions of individual counters, must be suitable to resolve the strongly forward-peaked multiplicity distribution of the reaction products.

The SLAC Crystal Ball[2]) design was adopted, which is based on the geometry of an icosahedron: a 20-faced solid figure in which each face is an equilateral triangle of the same dimensions. Each face is divided into 36 triangles, resulting in the division of the surface into 720 triangles, with only 11 different two-dimensional shapes. For the Plastic Ball modifications were made in details of the entrance and exit ports. Modules in the backward cone between $160^\circ$ and $180^\circ$ and in the forward cone between $0^\circ$ and $10^\circ$ had to be omitted in order to allow room for the beam pipe and prevent the beam halo from hitting the detector modules.

A further modification was necessary for the region between $10^\circ$ and $30^\circ$ in order to guarantee good particle identification despite the high multiplicities expected at forward angles. This region (known as the Mall) is subdivided into 160 modules instead of the 40 in the original design and positioned at a larger radius from the target position. This final geometry was chosen based on the results of Monte Carlo calculations using earlier measurements of multiplicity distributions[1]). In fig. 2 the probability for single hits in the Plastic Ball geometry is plotted (dotted line) versus the event multiplicity. As an example, for a multiplicity of 100 particles, the Plastic Ball will have typically 92 detectors fire, out of which 84 will have seen a single particle only.

The geometrical relationship between the triangular detector faces of the Plastic Ball, unfolded in a plane, is shown in fig. 3. The central spherical cavity of the ball has a radius of 25.4 cm, the outer radius is 61.4 cm. The aforementioned surface division scheme is applied to both the outer and inner surfaces. For assembly and access to the target, the ball is divided into two half-spheres along the $\theta = 90^\circ$ plane. A thin sheet of 1.2 mm steel with a hole 50 cm in diameter forms the baseplate of each hemisphere.

## 2.2 INDIVIDUAL DETECTOR MODULE

### 2.2.1 General Characteristics

Each of the 815 detector modules represents a particle identifying telescope with a $\Delta E$ and E detector using a slow and a fast scintillator read out via one photomultiplier[3]) (fig. 1). The $\Delta E$ counter is a $CaF_2(Eu)$ crystal[4]) with a characteristic decay time of 1 $\mu$s for the emission of the scintillation light. Unlike NaI the $CaF_2(Eu)$ is not hygroscopic and therefore needs no bulky canning, which would have jeopardized the system goal of a total coverage of $4\pi$

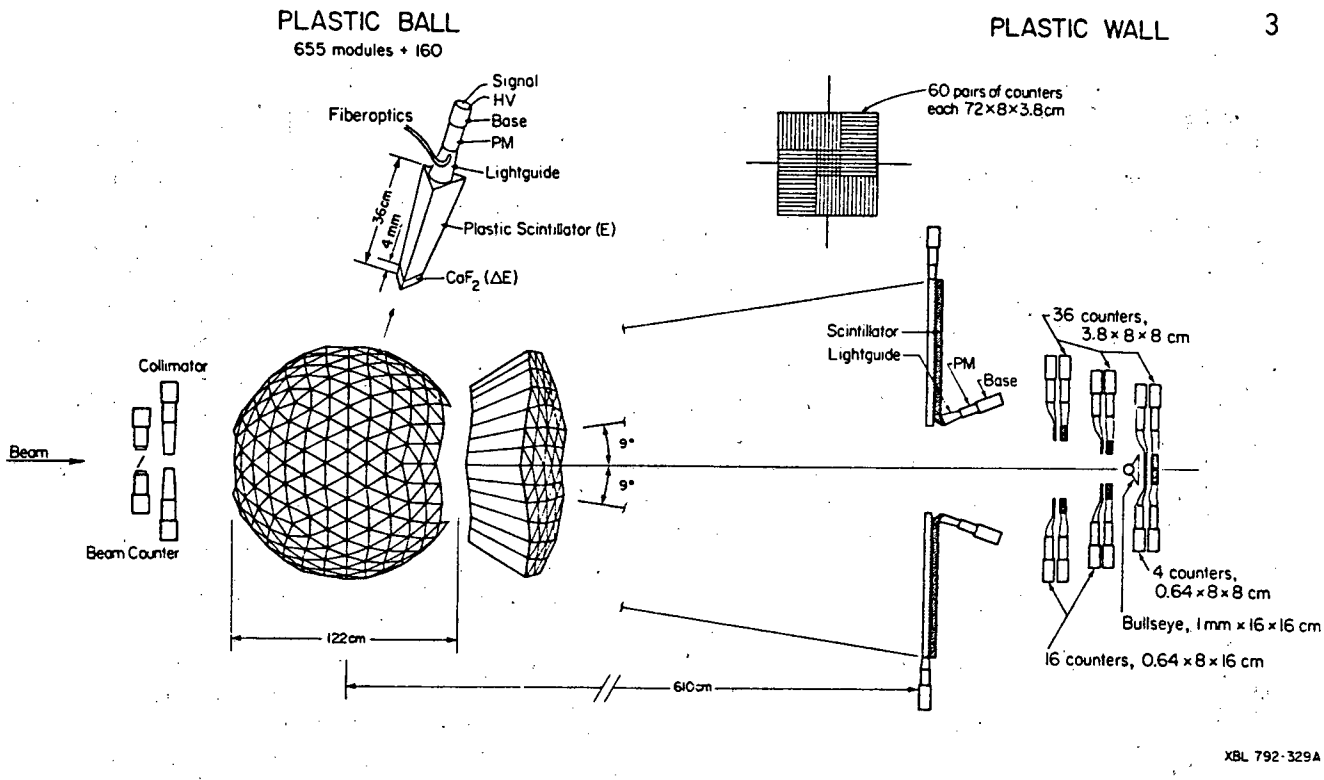


Fig. 1. Schematic view of the Plastic Ball and the Plastic Wall.

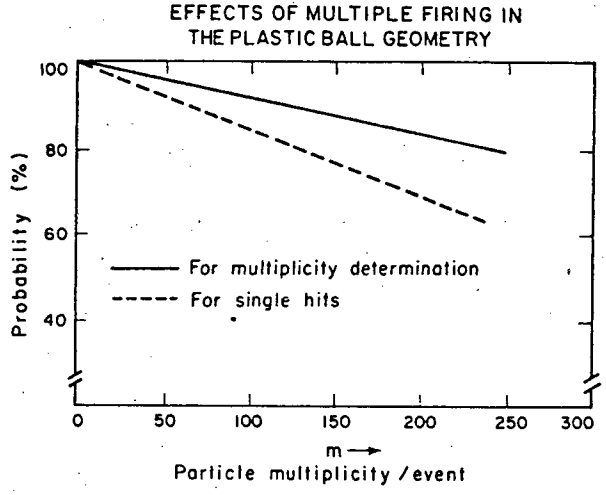


Fig. 2. Probability for single hit of a Plastic Ball module as a function of multiplicity.

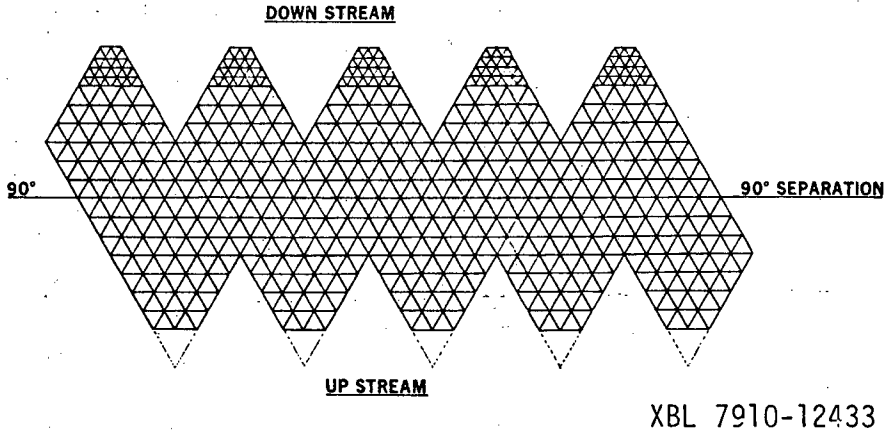


Fig. 3. Mercator projection of the Plastic Ball.

of solid angle. Each module is only wrapped with a double layer of aluminized mylar foil as an optical separator between adjacent modules. The light output of $CaF_2$ compared to that of anthracene is 100 to 120% and the crystal is extremely free of afterglow compared to NaI. The ΔE light is read out through the E counter (i.e., the E counter serves as a lightguide to the ΔE counter), which consists of a plastic scintillator[5]) with about 45% of the light output of anthracene. The light emission of the plastic scintillator is approximately 100 times faster than that of the $CaF_2$(Eu) so that 90% of the E signal is collected within 10 ns. Such a big difference between the time characteristics of the two scintillators is desirable because the plastic scintillator has, besides the dominant short decay time, some components with long decay times, which result, after 120 ns, in a pulse height ratio of only 1000:1 between fast and slow plastic decay components, but in ratios of about 10:1 for integration of the fast and slow components. This determines our choice for the onset of light collection for the ΔE signal, which is affected by these long decay times from the plastic scintillator. An optimum has been found for the ΔE-E resolution when the ΔE light integration lasts for 1.5 μs and starts about 240 ns after the start of the E signal.

The thickness of the ΔE $CaF_2$(Eu) crystal was chosen to be 4 mm with 35.6 cm as the length of the E plastic scintillator. This allowed good ΔE signals even for minimum ionizing particles and also a minimum low energy cutoff for particles stopping in the ΔE counter. In order to obtain clean proton spectra up to 200 MeV, the detector length was chosen to stop 240 MeV protons. This additional length assures that in the ΔE-E diagram the punch through deuterons do not disturb the proton spectra below 200 MeV. It also allows some toleration of dead zones in the outer corners of the modules, where mounting studs for the assembly were placed. The total length chosen represents a physical upper limit for particle identification for stopped particles due to the onset of reaction losses.

The readout of the ΔE-E module is done via a conically shaped lightguide (lucite), which couples to a 2-inch, 10-stage photomultiplier[6]). The phototube was selected for good gain and high linearity up to the high currents that are necessary for the subsequent pulse shape analysis. The gain of the phototube is monitored by a light pulse fed into the light guide via an optical fiber[7]) from a pulsed Xe-light flasher.

2.2.2 Neutron response

Since plastic scintillators are efficient neutron detectors, the effects of neutrons emitted in coincidence with a charged particle into the same detector module need to be considered to avoid misleading results in particle identification and energy determination.

Calculations were performed[8]) for a module shape similar to a Plastic Ball module taking into account recent measurements of proton kinetic energy and angular distributions at Bevalac energies, neutron multiplicities, and neutron efficiencies of plastic scintillators[9]). The average deposited neutron energy turned out to be ~10 MeV for neutron kinetic energies between 100 and 800 MeV and was slightly lower for lower energy neutrons. Thus the angle averaged probability for single hits (see fig. 2) will be reduced from 84% (considering only charged particles) to 81% when neutrons are included in the example of a multiplicity 100 event. There is no effect of neutrons on altering the charge identifcation for Z = 1,2. However, the particle mass may be assigned incorrectly if the deposited neutron energy is comparable to the separation of the particle identification curves in the ΔE-E plot. For charged particle multiplicities of 100 about 2% of protons will therefore be misidentified as deuterons, 2% of deuterons will be shifted to tritons, and 1% of protons will be misidentified as tritons. The $^3$He and $^4$He identification suffers approximately 0.5 to 1% misidentification.

## 2.3 PION IDENTIFICATION

In designing the Plastic Ball, special care was taken to detect the positive pions. As the yield of the $\pi^+$ is only about 10% of the proton yield at beam energies well above the pion production threshold, in a pure $\Delta E$-E identification scheme the pions would be overshadowed by the background produced by heavier particles. Therefore, the $\pi^+$ are additionally identified by their delayed decay. Stopped $\pi^+$ decay into a $\mu^+$ and a neutrino with a mean life of 26 ns and a Q-value of 4.12 MeV. The $\mu^+$ subsequently decays into a positron and two neutrinos with a mean life of 2.2 $\mu$s. In this decay the $e^+$ is emitted with an energy of up to 53 MeV and produces therefore a signal that is easily detectable in the plastic scintillators, as schematically shown in fig. 4. A discriminator in the electronics (Ball Box) detects the occurrence of this second spike and a TDC measures the delay time. The TDC covers the range between 250 ns and 10 $\mu$s so that about 90% of all $\pi^+ \rightarrow \mu^+ \rightarrow e^+$ decays can be recorded, provided the $e^+$ deposits an energy greater than 1 to 2 MeV in the scintillator. This requirement accounts for an additional loss of a few percent of the pions. If the decay occurs during the integration time of the $\Delta E$-ADC (250 ns-1750 ns), the $\Delta E$ signal can be spoiled, as the positron energy can be much higher than the energy loss of the pion in the $CaF_2$ (typically 2-3 MeV). Therefore, a separate signal is given to a third ADC, called $\Delta E_S$, with a shorter gate (700 ns) so that, depending on the time of the decay, one or the other $\Delta E$ signal or a combination of both can be used to extract the $\Delta E$ information.

This method can not be used to detect negative pions, as the $\pi^-$ are promptly absorbed by a nucleus in the detector and the 140 MeV rest mass of the pion is released as kinetic energy. The efficiency for $\pi^+$ detection was studied in detail using a pion beam at LAMPF. At very high incident energies this scheme can be used for $K^+$ detection.

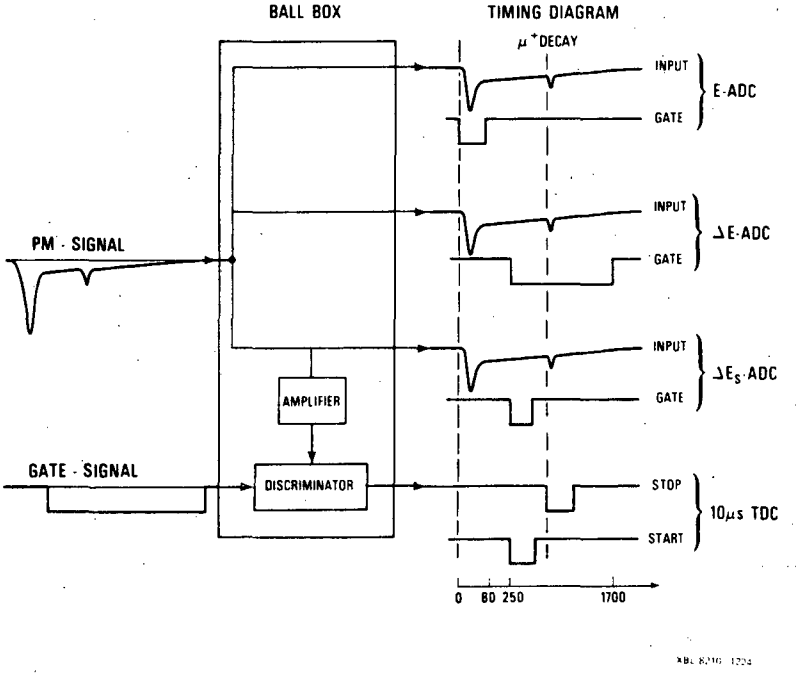


Fig. 4. Scheme of the pulse shape analysis of the signal from the Plastic Ball detector for $\pi^+$ particle identification.

## 2.4 GAIN MONITOR XENON STROBE SYSTEM

A xenon strobe flash tube system was adapted from a design used on the Stanford Crystal Ball[2]) to provide a monitor of the gains of the phototubes in the Plastic Ball. Eight flashers, each coupled to a bundle of about 100 light fiber cables[7]), deliver light pulses to the 815 phototubes. A silicon PIN photo diode[10]) in each flasher module records the pulse by pulse amplitude. During the beam spill the eight flasher modules, together with the wall pulsers are triggered cyclically with a 16-output-pulse-sequencer driven at a rate proportional to the counting rate in the beam start detector.

# 3. The Plastic Wall

The Plastic Wall (Pilot F) covers an area of 192 cm x 192 cm and provides fine position resolution coverage of the angular region between $\theta = 0^\circ$ and the forwardmost sections of the Plastic Ball ($\theta \sim 10^\circ$). It comprises two sections of scintillators, the outer Wall and the inner Wall (fig. 1).

The outer Wall serves to extend the acceptance of the Ball-Wall system from $\theta = 10^\circ$ to $\theta = 2.5^\circ$ detecting particles in the same range of mass and charge as the Ball itself, but measuring velocity and Z instead of energy, Z and A as in the Ball. The inner Wall extends the angular measurement to $0^\circ$. Besides measuring light fragments like pions, hydrogen, and helium the inner Wall is used to observe heavier fragments (Li, B...), which have small velocities in the projectile frame. In addition, the centre region of the inner Wall makes up the event trigger in the first round of experiments.

## 3.1 THE OUTER WALL

The outer Wall region consists of 60 pairs of counters, each 72 x 8 x 3.8 cm, providing coincidence units sensitive to charged particles passing through both bars of a pair. Neutron and gamma background is rejected by this coincidence requirement.

A time resolution of 350 psec (FWHM) was achieved for minimum ionizing protons. The mean time of the pair gives the flight time from the target and hence the particle velocity.

Each scintillator signal is fed to an ADC, and Z identification is achieved (as suggested by the Bethe Block equation) by generating a function $v^2\Delta E$, where v is the measured particle velocity and $\Delta E$ is one of the two $\Delta E$ signals.

Corrections to the scintillator pulse height were necessary because of

a) attenuation of light along the length of the scintillator and
b) non-linearity at the end of the rear scintillator, due to the bent light guide.

Since the yield of fragments with $Z > 3$ was negligible the phototube gain was set so that heavy fragments caused an ADC overflow, hence they were counted but not identified. On-line gain monitoring was carried out with light from a $N_2$-laser.

Calibration of the position spectra was done by means of eight narrow (3.8 cm) bar scintillators mounted as a third layer, perpendicular to the length of the pairs at a fixed position from one end. By means of a threefold coincidence caused by particles passing through the mid-point of the pair and through the calibration bar, a position calibration was achieved to an accuracy of 2 mm.

## 3.2 THE INNER WALL

The inner Wall covered the region within $2^\circ$ of the beam and was finely divided because of the high multiplicity of fragments near the beam. Its main purpose was to form the fast trigger with the upstream beam counter and collimator to decide which events were to be recorded. Of course, it also gave

nuclear charge and velocity information for the particles it detected and could be used for centering the beam on the Wall.

The inner Wall consisted of a 6 x 6 array of 36 thick scintillators 8 x 8 $cm^2$ each, 3.8 cm thick. In front of each was a 0.64 cm thin scintillator. For the center four counters the thin and thick scintillators were of the same area and in one to one correspondence, but for the remaining 32 thick scintillators, only 16 thin scintillators were used, each 8 x 16 $cm^2$ in area and covering a pair of thick detectors. The 56 scintillators had light guides and phototubes coupled on one edge. In addition, in front of the center four pairs of scintillators was placed one 16 x 16 $cm^2$ "Bull's Eye" scintillator, only 1 mm thick. The purpose of the bull's eye was to reject beam particles, and it was made thin to minimize nuclear interactions in the detector itself. The Bull's Eye had light guides and phototubes coupled onto two opposite edges.

## 4. Upstream Beam Counter

The upstream counter is a thin plastic film scintillator with a projected diameter of 2.5 cm and together with an active collimator 3 m upstream defines the beam acceptance of the ball detector system. This counter establishes the timing reference for the fast trigger and also the start signal for the TOF measurement in the Plastic Wall. It was designed to have very low mass and also for optimal light collection in order to achieve good time resolution while minimizing the background from material in the beam. A sandwich of three scintillator films with a combined thickness of roughly 3.6 $mg/cm^2$ were supported in the beam at 45° on a stretched film of 0.275 $mg/cm^2$ (2.5 μm) hostaphan. The frame for this is a cylinder of aluminized mylar (125 μm), which doubles as a reflector. Two Phototubes (RCA 8575) view the scintillator from each end of the cylinder. A coincidence requirement between the two tubes eliminates a small background caused by beam halo striking a photocathode. The timing reference is extracted from the analogue sum of the two phototube signals with a constant fraction discriminator. The time resolution achieved between this detector and the inner Plastic Wall is 350 ps. A large area (30 cm x 30 cm) active collimator, which is sensitive to minimum ionizing particles, largely rejects nuclear interactions in the upstream thin film beam counter, which would otherwise be confused with target interactions. Although the rejection of beam in the active collimator is done on-line with hardware, the rejection of minimum ionizing particles is done using its TDC off-line so as not to reject particles coming backwards from the target.

## 5. Mechanical systems

The geometry chosen for the Plastic Ball made for convenient construction in two hemispheres, permitting easy access to the interior of the Ball for the target installation. The use of thin targets, required to avoid losses at large angles, made the construction of a full vacuum vessel mandatory to ensure that beam particles interact only in the target. Figure 5 shows the inside of the Plastic Ball with the 360 μm thick Am-vacuum chamber and the target wheel. Figure 6 shows the birds eye view of the fully assembled system.

## 6. Signal processing

### 6.1 GENERAL LAYOUT

Figure 7 schematically shows the layout of the electronics for the experiment. The event trigger is derived from the beam start counter and from the inner Plastic Wall detectors. Presently, the Plastic Ball is not involved in the trigger decision. Therefore, the signals from all 815 Ball modules are

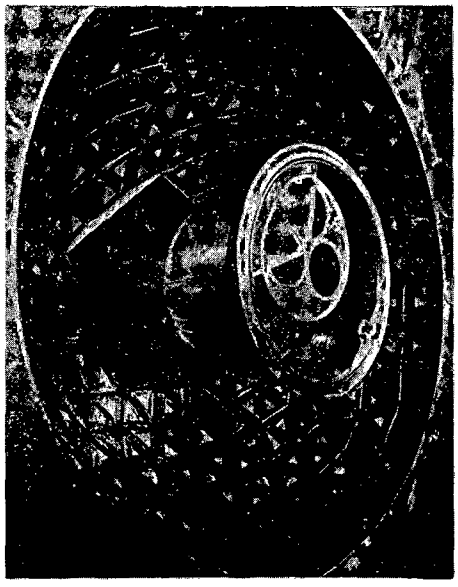

CBB 817-6532

Fig. 5. The downstream part of the scattering chamber with the target wheel installed into the forward hemisphere of the Plastic Ball.

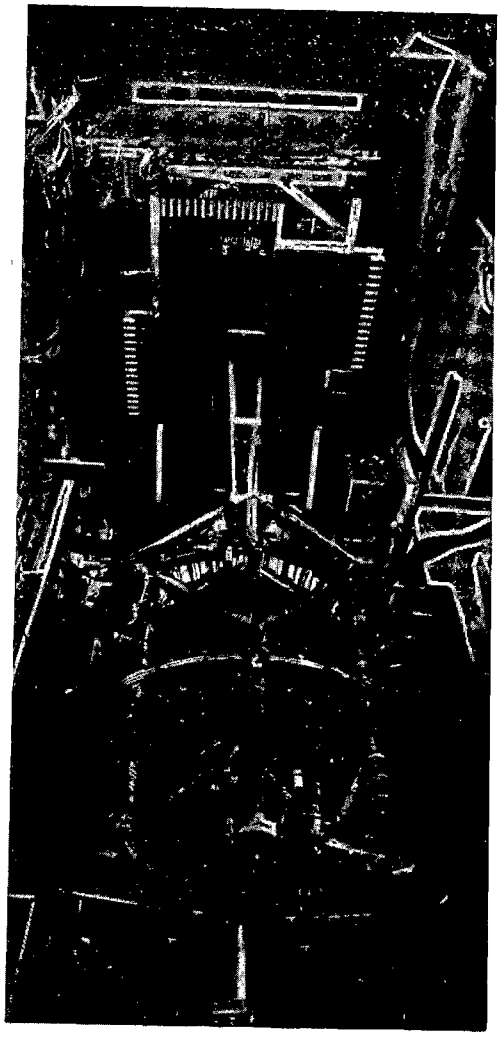

CBB 818-8088

Fig. 6. A view of the full system as installed at the Bevalac, looking downstream.

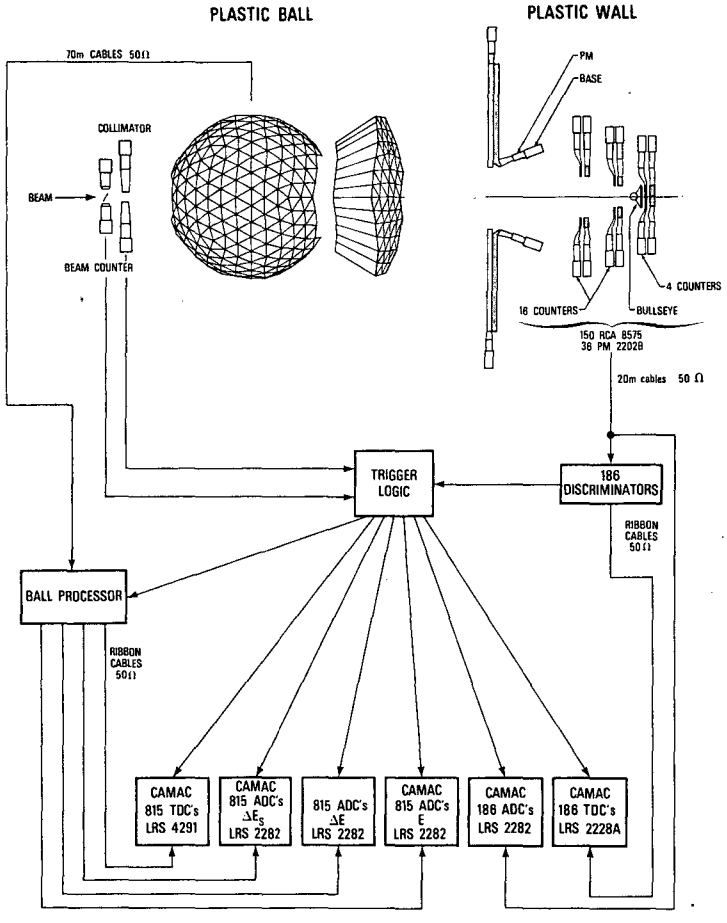


Fig. 7. Electronics layout.

delayed via 70 m cables (RG58) and fed into the Ball Box (see fig. 4) to allow time for the trigger decision, whereas the other counters have the shortest possible cables (RG 58) with a length of only 20 m.

A passive split generates three input signals for the E, $\Delta E_S$, and $\Delta E$ ADCs and one for an amplifier. The first three signals are fed via 25 fold 50-ohm ribbon cables to LRS 2282B ADCs. The fourth amplified signal is given to a discriminator and via twisted pair cables to LRS 4291 TDCs with a 10 μs range. The Wall signals are split in the octal constant fraction discriminators (Wall Box), and both analogue and logical outputs are given via 50 m long 8 fold 50 ohm ribbon cables to ADCs and 100 ns full-scale TDCs. The Inner Wall discriminator outputs are also used in the trigger logic described below. The Wall discriminator signals to the TDCs are regenerated just before the TDCs because of attenuation in the long cables.

### 6.2 TRIGGER

The time reference for the trigger signal is derived from the sum of the two photomultiplier signals of the start counter.

Beam particles that pass through the active collimator placed 50.5 cm downstream of the start counter veto the trigger signal. The discriminator on the summed collimator signal is set high, so that only beam particles, and not back scattered reaction products from the target, are vetoed.

The simplest trigger for high energy heavy ion studies is to require that the beam particle underwent a reaction between the beam counter and the Wall counters. This so-called "minimum bias trigger" is of great importance since all more restrictive trigger selections are normalized to it. After detecting a beam particle in the start counter, one demands that the projectile loses at least one charge.

During the first experiments the "central trigger" used required that no beam velocity particles of proton pulse height or higher were recorded in the inner Wall.

### 6.3 GATES

The live trigger signal is used to produce the different gate signals for the ADCs--the essential part of pulse shape analysis for particle identification--and the start signals for the TDCs and also to start the data conversion and readout. The timing for the ADC and TDC gates is shown in fig. 4. The Ball E-ADCs are gated with prompt 80 ns pulses to allow only the conversion of the short fast rising plastic scintillator signal. The gates for the two $\Delta E$-ADCs are both delayed by 240 ns and have lengths of 700 and 1500 ns, respectively. The discriminators in the Ball processors receive a gate of 10 μs length that is also delayed by 240 ns to suppress the prompt signal from the plastic scintillator and to produce a signal only for a delayed $\mu^+$ decay. The Wall ADCs have prompt, rather broad gates (120 ns) to allow for variations in the time of flight of the reaction products reaching the Wall.

## 7. On-Line data handling

The torrent of information coming from the Plastic Ball and the Plastic Wall requires sophisticated early inspection and selection in order to restrict the data flow to the significant data. "Smart" readout processors were applied in the Camac branch and a microprocessor was used for other Camac modules. One PDP-11/50 processor was dedicated for data collection and writing on tape while a second PDP-11/44 was used for on-line analysis of the data. All data produced by an event are converted and read out by Camac modules. The E, $\Delta E$, and $\Delta E_S$ analogue signals from the Plastic Ball are fed via mass terminated ribbon cables into 48 fold LRS 2282 ADC modules. The $\mu^+$ decay times (from the $\pi^+ \rightarrow \mu^+$ decay) are measured over a range of 10 μs with 32 fold LRS 4292 TDCs, and all

wall counter times are recorded with 8 fold, high resolution LRS 2228A TDCs. There are a total of 2631 ADC channels, 817 long-range TDC channels, and 188 high resolution TDCs.

Since for each event only a few hundred modules carry valuable information, a "smart" readout system is used to avoid a huge amount of useless data words. It was primarily this requirement that led to the choice of the commercially available LeCroy ADC and TDC systems.

The Camac system is interfaced to the on-line computer with a BIRA microprogrammed branch driver (MBD).

## 8. Calibration and performance

### 8.1 $\pi^+$ CALIBRATION AT LAMPF

To study the geometrical properties of the modules and to gain information on how well the particle identification scheme would work, an experiment was performed at the Low Energy Pion Beam (LEP) at LAMPF.[11])

An assembly of 13 Plastic Ball modules was placed in the beam defined by two 2 x 2 cm scintillation counters. Different kinds of particles with the same momentum (pions and protons) were selected by setting appropriate windows on the time-of-flight spectrum between those two counters. Thirteen modules were used and arranged such that the central module is completely surrounded by all possible neighbours as shown in the front view in fig. 8. This configuration specifically permits the study of the two dominant effects determining the detection efficiency: a) the scattering out of particles during the slowing down process and b) the detection probability for the positrons stemming from the $\pi^+ \rightarrow \mu^+$ decay. (These positrons are emitted isotropically with a maximum energy of 53 MeV and have a high probability of leaving the module). Both effects make it necessary to take information in the neighbouring modules into account in order to reconstruct the event. By having particles impinge on the module in the three different points (center point, side of two modules and corner of six

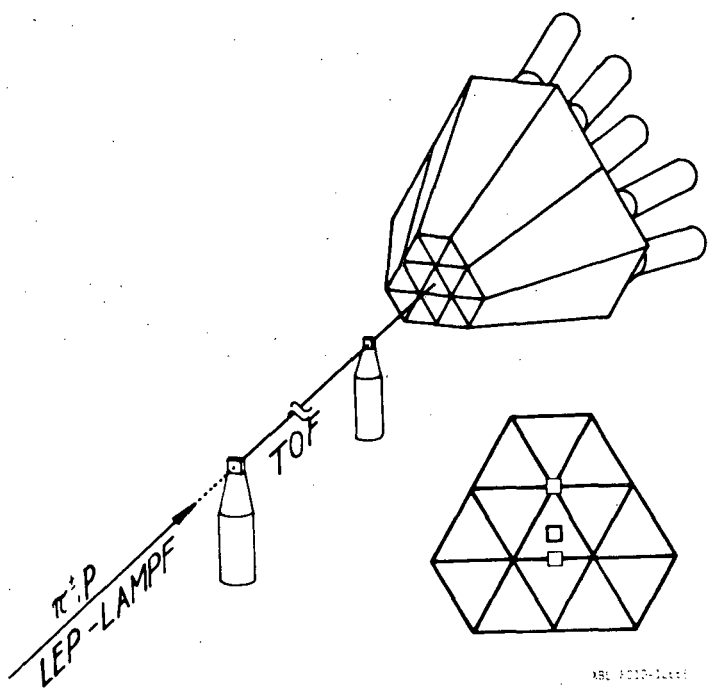


Fig. 8. Experimetal setup at the low Energy Pion Channel at LAMPF. The squares in the righthand front view indicate the three different entry points studied.

modules), the dependence of the reconstruction efficiency on the geometrical entry point can be determined.

A comparison of the detection efficiencies measured for the three different entry points into the module assembly yields the gratifying result that nearly all scattering out can be reconstructed.

A very important task of the test was to obtain energy calibration curves for pions and protons. For the energies covered by the measurements at LAMPF (low energy part for protons and high energy part for pions) the light output is surprisingly linear with energy. This was not expected, since the geometrical light collection along the particle path as measured on the surface with an electron source is not constant, the light collection near the $CaF_2$ crystal being about a factor of 2 better than near the phototube.

The measured detection efficiency for pions is given in fig. 9. The solid curve indicates the probability of measuring a decay time in the range between 200 ns and 10 μs. Theoretically, this probability is 90% and is independent of energy. Due to the positron discriminator threshold at about 4 MeV and the fact that the continuous positron spectrum extends below that energy, only 80% of the pions can be tagged at low energies. (The final discriminator setting is at ~1.5 MeV thus improving this number.) However, this number decreases at higher energies because a) more pions are lost due to reactions, b) the stop point of the pions is closer to the end of the scintillator where the light collection is lower (due to the geometry of the detector) and the probability for positrons escaping the counter system without giving a detectable signal increases. The dashed line in fig. 9 shows the measured probability of detecting a pion within the same decay time and also with an energy within 10% of the incident energy. Both efficiency curves have been corrected for accidental stops in the TDCs. The number of accidentals can be determined as the flat background under the exponential decay curve.

## 8.2 CALIBRATION AT THE 184" CYCLOTRON

After assembly each individual module of the Plastic Ball was calibrated at the Berkeley 184" cyclotron with 800 MeV and 400 MeV α beams. This procedure allowed the determination of the proper high voltage for each individual photomultiplier and of an important constant for each module, the ratio of E to ΔE pulse heights at a given energy. In addition, the energy calibration for the hydrogen and helium isotopes was obtained by observing the fragmentation products of an 800 MeV α beam hitting a thick target and by measuring the time of flight of the products in front of the module. The E calibration for α-particles was obtained by varying the energy of the incident α beam with moderators in steps of 100 MeV.

The relation between measured pulse-height and deposited energy is shown in fig. 10 for p, d, $^4$He, and positive pions. Immediately after the irradiation each module was cross-calibrated with a calibrated Xe-flasher. After the assembly of the Plastic Ball each module was calibrated again with the same flasher, and thus all information from the calibration measurements could be related to the actual experiment.

## 8.3 PERFORMANCE

### 8.3.1 Plastic Ball

The tests performed at the LAMPF low energy pion beam line and at the Berkeley 184" cyclotron with 800 MeV α particles showed that the energy resolution of a single module is sufficient to achieve the desired particle identification. The following energy resolutions (FWHM) were measured: for 75 MeV protons the plastic scintillator (E signal) had a resolution of 5% and the $CaF_2$ crystal (ΔE signal) of 12% respectively. For the 800 MeV α beam the figures were 2% for the plastic scintillator and 10% for the $CaF_2$.

The first Bevalac experiment was performed in June 1981 with a 800 MeV/u Ne beam on a Pb target and $^{40}$Ca beams at 400 MeV/u and 1.05 GeV/u on a calcium

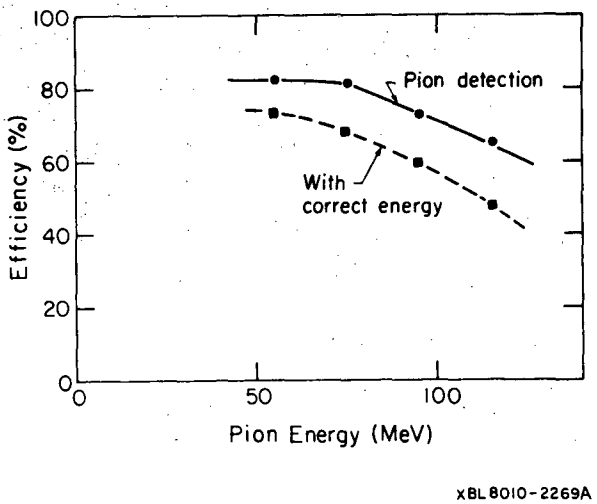


Fig. 9. $\pi^+$ detection efficiency (solid curve) and detection efficiency with correctly (within 10%) measured energy (dashed curve).

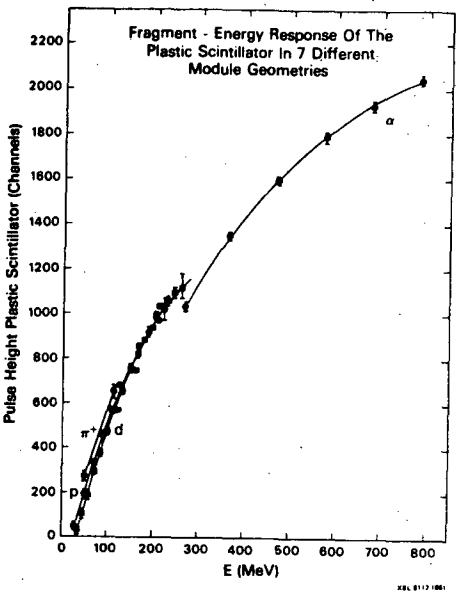


Fig. 10. Response of the plastic scintillator in the Plastic Ball detector geometry to the energy of $\pi^+$, p, d, and $^4$He.

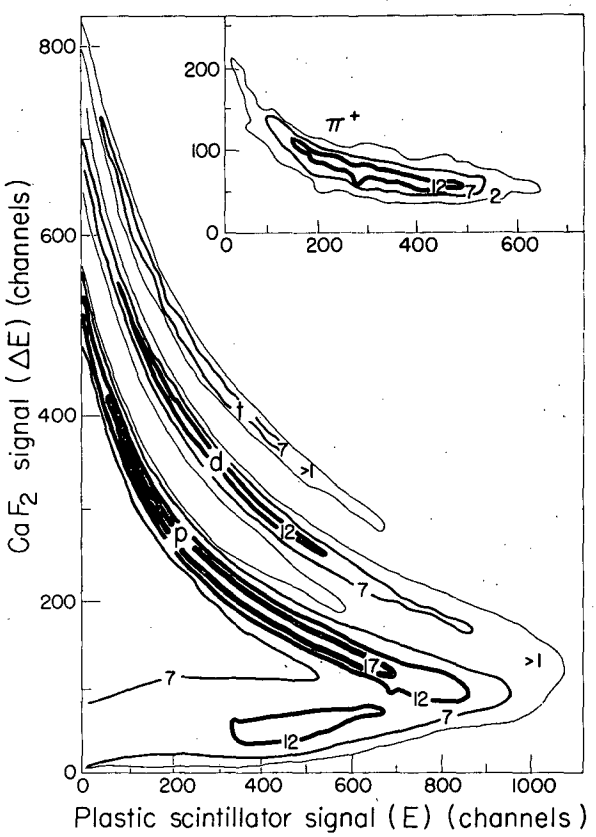


Fig. 11. ΔE-E contour diagram of 655 modules after gain matching and scattering out reconstruction of approximately one million reaction products. The contour lines are labeled as to their relative height in arbitrary units. The upper contour diagram for $\pi^+$ is obtained by requiring a delayed decay signal measured in the 10 μs TDCs.

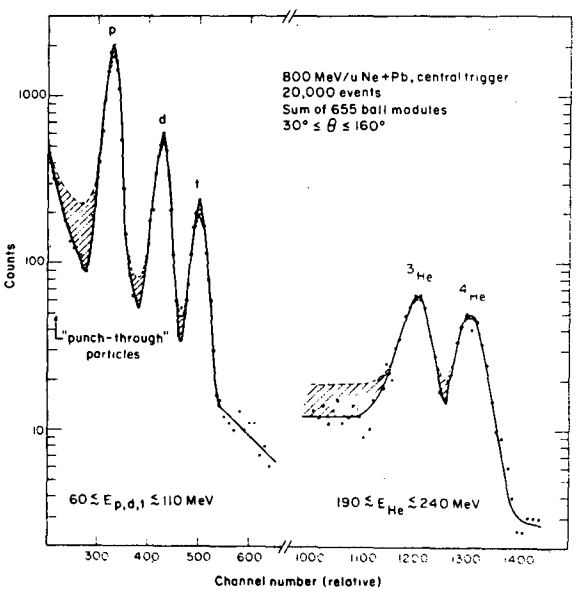


Fig. 12. Particle identification spectrum for 655 modules after gain-matching and with and without scattering out reconstruction.

target. From the actual data and from the calibration measurements, correction factors for the ΔE and the E pulse heights could be derived in order to achieve the proper gain matching for all modules. The quality of the particle identification for the 655 modules between 30° and 160° is shown in fig. 11. A cut in the ΔE-E plane perpendicular to the particle identification lines is selected with ΔE and E projected on this cut in a certain energy range. The integrated yield is shown as a function of this projection in fig. 12. The dashed curve represents the raw data after gain-matching, whereas the solid line shows the particle separation after all scattered out particles have been reconstructed by taking into account up to 12 neighboring modules that surround a center module and that contain only E but no ΔE information. Windows were selected along the valleys of those distributions allowing one to assign a mass and charge value with high confidence. For the particular case of 800 MeV/u Ne on Pb and a central trigger configuration, 35% of all detected tracks fall into a particle identification window, 22% of those being stopped in the plastic scintillator and 13% being high energy particles that do not stop in the detector and give only Z information. 13% of all particles have very low energy and stop in the 4 mm thick $CaF_2$ crystal, where only energy can be measured but no mass or charge. In 47% of all detected tracks only an E but no ΔE signal is present. These are presumably neutral particles (mostly neutrons) interacting in the scintillator; however, scattered out particles unaccounted for in our reconstruction algorithm may also give the same signature. For 5% of the detected tracks a ΔE and an E signal are obtained, but an assignment to a defined particle is not possible. These cases are due to double hits and reaction losses in the scintillators.

In the ΔE-E contour plot (fig. 11) the pion branch coincides partly with the punch through hydrogen branch and pions can only be identified by taking information from the decay measurement into account. Figure 13 shows the decay curve for the identified positive pions. The solid curve is a fit of the experimental decay with the decay constant of 2.2 μs and a constant background that indicates that only 3% of all pions are misidentified.

8.3.2 Plastic Wall

Since the Plastic Wall can detect beam velocity particles the time calibration is taken from each individual experiment. In the 800 MeV/u $^{20}Ne$ on Pb experiment a time resolution of ~350 ps was observed between the inner Wall detectors and the beam counter. The pulse height resolution of the Inner Wall was good enough to have Z-identification up to the projectile Z of ten. For the Outer Wall, where dominantly hydrogen and helium fragments are detected, a pulse height resolution of ~20-25% was good for an excellent separation of hydrogen, helium, and lithium.

These performance figures of the Ball and the Wall allow one to draw a figure for the system's response as a function of fragment momentum and rapidity. Figure 14 shows the response of the Ball and the Wall for protons or α-particles. The curves for deuteron, tritons and $^3He$ are slightly different, with deuterons and tritons lying at smaller $p_\perp$ values and $^3He$ at larger $p_\perp$ values than for the protons.

## 9. Physics with $4\pi$ data

The beauty in $4\pi$ data is that nearly the whole physics is contained in each event. But as with so many (sleeping) beauties, thorny hedges surround them and huge efforts are needed to set them free.

Most of the early attempts with AgCl and emuslion detectors used the $4\pi$ feature to extract angular distributions for specific event selections. The streamer chamber groups went one step further and studied $\pi^- - \pi^-$ (two particle) correlations to learn something about the size of the reaction volume. However, visual detectors have their strength in showing sparkling stars that strongly stand out from the average.

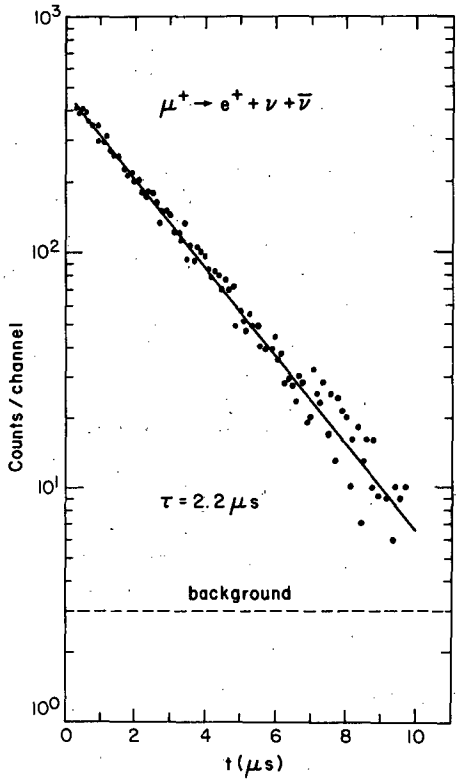


Fig. 13. Time spectrum of delayed coincidences of 655 detectors. The straight line is a best fit yielding a proper decay time of 2.2 μs with a 3% background.

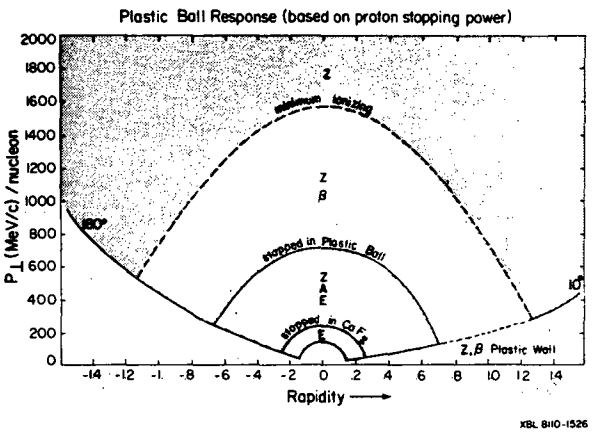


Fig. 14. Plastic Ball and Plastic Wall response in the transverse momentum $p_\perp$ versus rapidity y plane. The limits labeled "stopped in $CaF_2$" and "stopped in Plastic Ball" refer to protons and $^4$He fragments; those for d, t are lower but somewhat higher for $^3$He fragments.

Here, using the Plastic Ball data, a few attempts will be discussed to study one of the most fundamental question of relativistic heavy ion physics, "Do relativistic nuclear collisions allow to study the equation of state of nuclear matter?"

Because in single particle inclusive data the averaging occurs over impact parameter and multiplicity, all viewpoints on the reaction mechanism extracted so far are questioned until found in agreement with these new $4\pi$ data.

We will focus onto three subjects and their beauties (in parentheses)

1) Cluster formation (Entropy)
2) Thermalization (Temperature)
3) Flow (Density)

## 9.1 CLUSTER FORMATION

Recently it was pointed out that the entropy production can be related to the cluster production, especially to the ratio of deuteron-to-proton yield[12]), i.e., the larger this ratio the smaller the entropy produced in the reaction. This has stimulated a large dispute in the theory community[13-18]) of whether this is at all possible or how to construct the right observable from cluster production cross sections. If one really could measure in this way the entropy then one could look for the predicted change in entropy as the dense nuclear matter undergoes, as it were, a phase transition.

This focuses onto the mechanism of cluster production. In one of our early theoretical adventures we formulated the nuclear coalescence model to describe the observed cluster production.[19]) Basically, it states that two nucleons have to be close in phase space to have a chance to coalesce. In the first formulation the nucleons had to be close only in momentum space but there is of

course also a requirement that they are close in configuration space to interact in one short time interval. With $\vec{p}_1$ and $\vec{p}_2$ the momenta of particles 1 and 2 and $\vec{r}_1$ and $\vec{r}_2$ the coordinates in configuration space, one requires for coalescence

$|\vec{p}_1 - \vec{p}_2| < p_o$ and--usually neglected!-- $|\vec{r}_1 - \vec{r}_2| < 2r_o$

$|t_1 - t_2| < \Delta t_o$

Then $\frac{\sigma_{deuteron}}{\sigma_{proton}^2} = \frac{4\pi}{3} p_o^3$ .

If we assume a thermal equilibrium (as in a fireball) then Mekjian[20]) has shown that the volume V of the emitting source can be obtained via $\frac{4\pi}{3} p_o^3 = \frac{8}{\gamma} \frac{(2\pi)^3}{V}$ where $\gamma$ is the Lorentz factor of the emitted particle in the center of mass frame of the fireball (at the energies discussed $\gamma \approx 1$). From single particle inclusive data[21]) this volume seems to increase as the mass of the target increases but, e.g., for $^{20}$Ne + Pb does not change with bombarding energy. We can now employ for the first time $4\pi$ data in this context. Because of the Plastic Ball's particle identifying feature, one can study the cluster production as a function of event multiplicity in each event. Furthermore, a comparison is possible of the deuteron to proton ratio versus the deuteron-like to proton-like ratio as suggested in ref. 5. with:

$$n_{deuteron\text{-}like} = n_d + \frac{3}{2}(n_t + n_{^3He}) + 3\, n_{^4He}$$

$$n_{proton\text{-}like} = n_p + n_d + n_t + 2\,(n_{^3He} + n_{^4He})$$

For the investigation of entropy it is of importance to compare protons and clusters originating from the same volume of phase space. It has been reported[22] that in the $^4$He spectrum (e.g., 2.1 GeV/u $^{20}$Ne + Au), there is a large cross section of up to 13b at very low $\alpha$-energies due to an $\alpha$-particle production at a very late state in the reaction when the fast particles have left the reaction zone. It is our opinion that this late state has to be excluded in this study and to do this in an adequate way a low-energy threshold has to be applied to the data. We have chosen for all particles a threshold of E/A = 40 MeV. Such a low energy cutoff should be incorporated into theoretical comparisons since values obtained this way for ratios of deuteron-like/proton-like are lower than those extracted using the full spectrum. Furthermore, this study limits data to emission angles of $9^\circ \leq \theta \leq 160^\circ$ ignoring the small yield of particles going into $0^\circ$ to $9^\circ$. This forward region contains dominantly projectile-spectator residues for large impact parameter reactions. As we will stress the high multiplicity events, this region is not affecting the results.

Figure 15a shows the deuteron-to-proton ratio for Ne + Pb at 800 MeV/u as a function of the charged particle multiplicity $M_c$ in the event. There is a steep rise of d/p up to a value of 0.3. These data point out that the deuteron production increases the more nucleons are involved in the reaction. Figures 15b and 15c show for the same reaction the ratio of deuteron-like to proton-like particles. Notice the larger values compared with d/p and a more pronounced saturation at high $M_c$. Figures 16a and 16b represent these ratios for the reaction of 400 MeV/u $^{40}$Ca on Ca.

Can the increase in deuteron production with increasing multiplicity be understood in terms of the current models for cluster production? In the thermal model assuming chemical equilibrium[23]) the ratio of d/p was independent of the size of the thermal source, and d/p as a function of M was expected to be constant. In the original coalescence model[19]) the size of the participant volume was neglected and the coalescence volume in momentum space was taken as proportional to the inverse of the size of the deuteron. This predicted that $d/p^2$ as a function of multiplicity (not d/p) was expected to be constant.

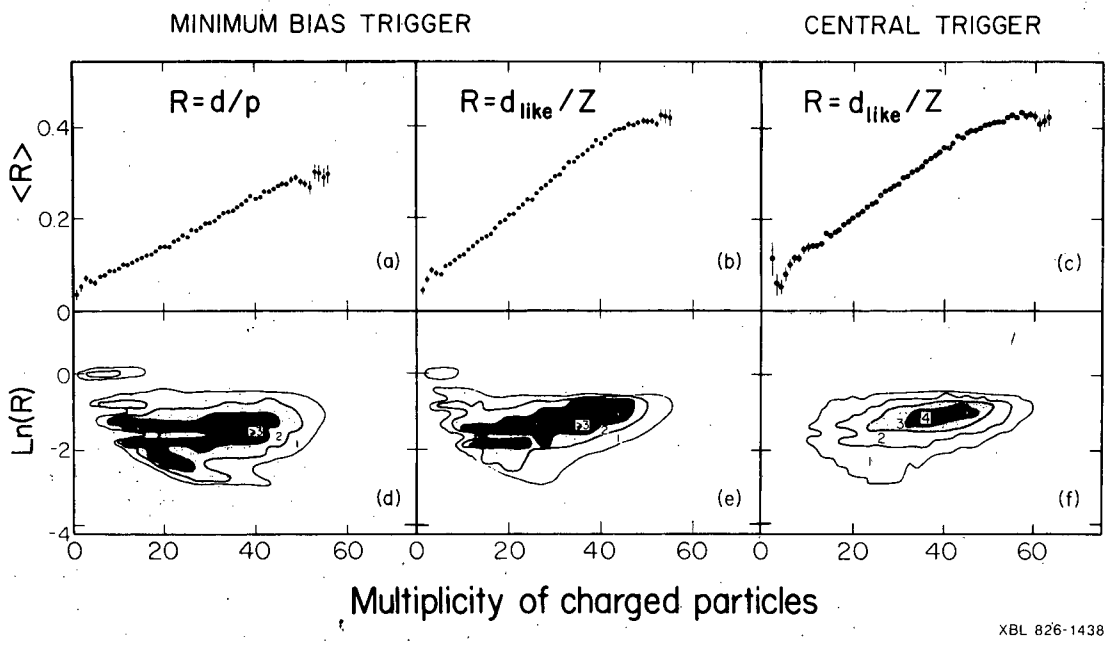


Fig. 15. a,b,c: Ratio of deuteron to proton production (a) and ratio of deuteron-like to proton-like particles with two different trigger conditions (b,c) as a function of the total observed charged particle multiplicity for the reaction 800 MeV/nucleon Ne + Pb

d,e,f: Corresponding event by event contour plots of the logarithm of the ratio versus the charged particle multiplicity. Relative intensities are indicated by the contour lines.

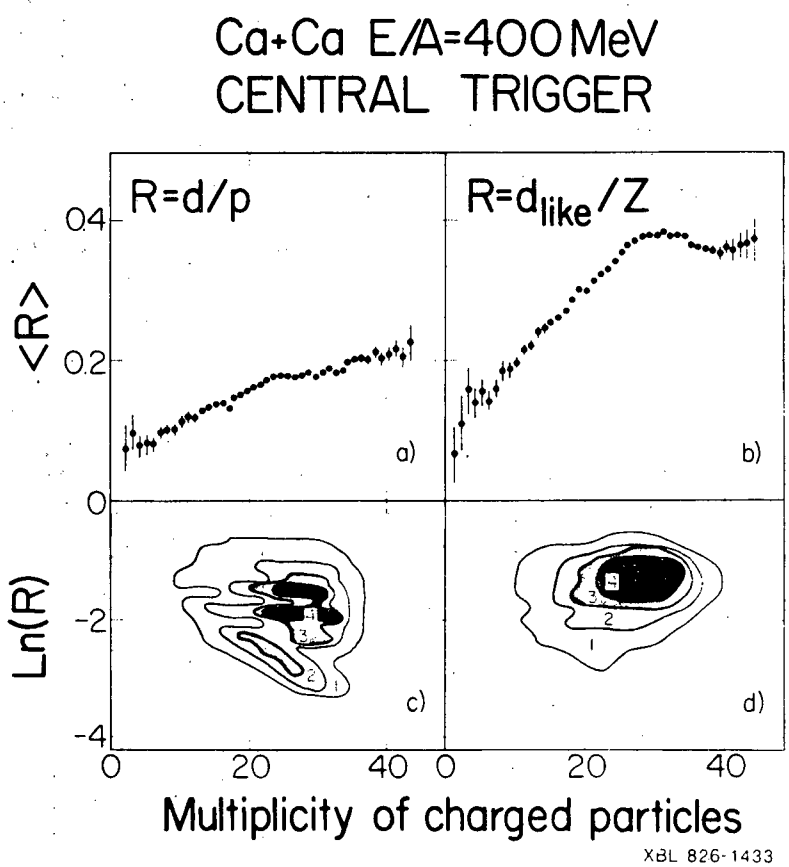


Fig. 16. Same as fig. 15 but for the reaction 400 MeV/nucleon Ca + Ca.

Jennings et al.[24]) have shown the practical equivalence of the coalescence and thermal models. If one introduces into the coalescence model the volume of the deuteron in configuration space and integrates over the number of particles, this produces a term proportional to the volume of the participants as in the thermal model. Recently, Sato and Yazaki[25]) have formulated a model taking into account both the size of the deuteron and the volume of the participants. The coalescence radius $p_o$ in momentum space is related to the deuteron radius $r_d$ and that of the participant volume $r_p$ via

$$\frac{d_{like}}{p^2_{like}} = \frac{4\pi}{3} p_o^3 \propto \frac{1}{(r_d^2+r_p^2)^{3/2}} \quad .$$

The deuteron radius $r_d$ is an average over the clusters used in the definition of $d_{like}$. The radius $r_p$ of the participant volume can be related to the observed charges by

$$r_p = r_o \, (2 \, p_{like})^{1/3}$$

with $r_o$ a free parameter (since the participants are most probably not in a compact sphere). For the $d_{like}$ to $p_{like}$ ratio one finds

$$\frac{d_{like}}{p_{like}} \propto \frac{p_{like}}{(r_d^2+r_o^2(2p_{like})^{2/3})^{3/2}} \quad .$$

Figure 17 shows the ratio $d_{like}/p_{like}$ as a function of $p_{like}$. The solid line is a fit to the data drawn with $r_d/r_o = 2.6$. By neglecting one or the other of the terms in the denominator one can obtain both limiting behaviors described above. If the volume of the deuteron were neglected the line would be horizontal; on the other hand, if the volume of the participants were neglected, the line would be linear through the origin. Therefore, to extract valuable information on entropy one has to know the variation with multiplicity. Entropy values from single particle inclusive data may be meaningless because they integrate over all impact parameters.

Data with a central trigger are shown in fig. 15c for comparison with the minimum bias data (fig. 15b). They practically overlap proving that the central trigger is not producing a special bias in the cluster production but only an enhancement of high multiplicity events.

Figures 15d,e,f and 16c,d show the ratio of d/p and of $d_{like}/p_{like}$ in each event as a contour plot. Each plot contains approximately 140 000 events. Focusing on the central trigger data (Figs. 15f and 16d), one observes a depletion of low multiplicity data as expected. A comparison of the contours in d/p versus those in $d_{like}/p_{like}$ shows a narrower distribution for $d_{like}/p_{like}$, supporting the choice of these variables in the analysis. The largest ratios are almost as large as those that would be calculated by Bertsch and Cugnon[15]) for zero impact parameter collisions, but it must be remembered that the 40 MeV/u cutoff has not been put in the theoretical calculation. However, these authors predict a decrease in entropy with decreasing impact parameter, which in turn would predict an increase in cluster production with increasing multiplicity, as observed in our data. In ref. 5 this increase of entropy is explained by the smearing of the participant volume by the mean free path of the nucleons, which may be equivalent to including the finite size of the deuteron. In fact, Biro et al.[17]) found they had to include the volume of the deuteron in their thermal model.

## 9.2 THERMALIZATION

One huge step towards the equation of state would be a clear signal of thermalization in the primary reaction zone. In the late state of the reaction an apparent temperature of ~20 MeV seems to be clearly established and is discussed in association with the boiling or condensation point of nuclear matter.[22]) The nuclear fireball was introduced with the assumption of total thermalization among the participants whereas the hydrodynamical model[26])

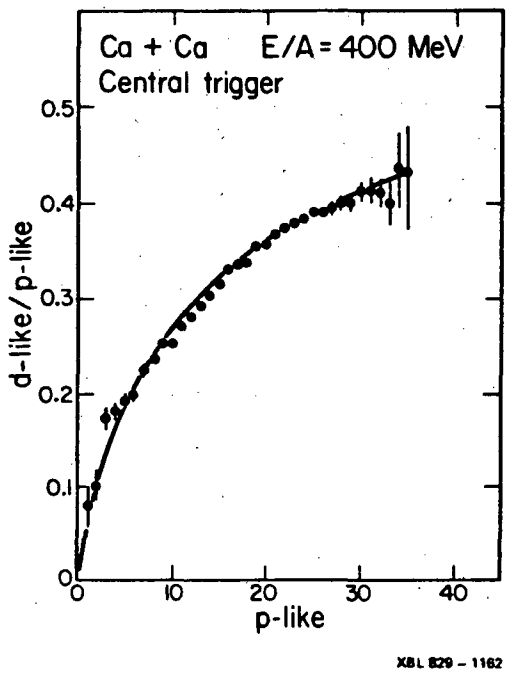


Fig. 17. Ratio of the number of deuteron-like to proton-like particles as a function of the number of proton-like particles. The solid curve represents a fit to the data.

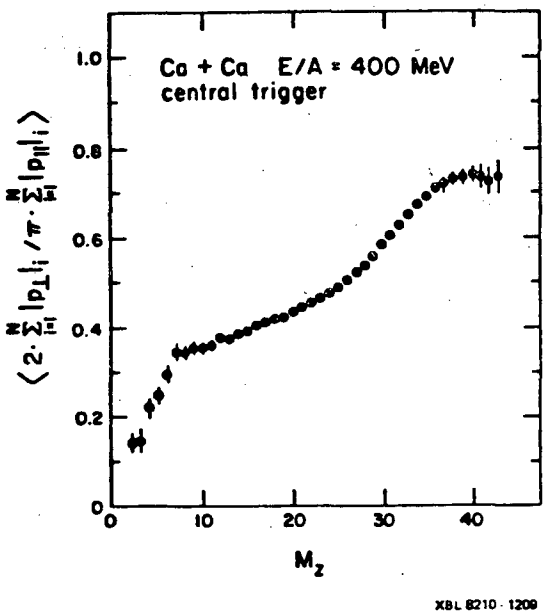


Fig. 18. Ratio of $2\cdot\sum|p_\perp|_i \Big/ \pi\cdot\sum|p_\parallel|_i$ as a function of nucleonic charge multiplicity averaged over 50 000 events. A value of 1 would correspond to a completely thermalized event.

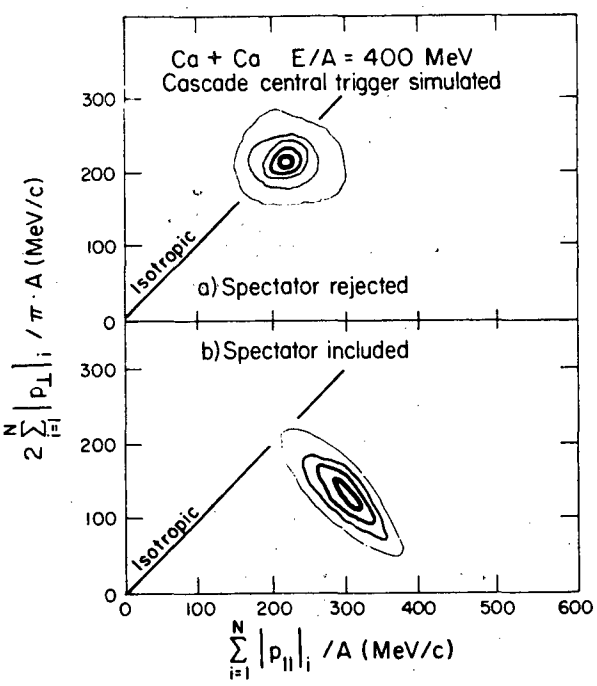


Fig. 19. Contour plot of $\langle p_\perp/A \rangle$ versus $\langle p_\parallel/A \rangle$ for a cascade calculation Ca on Ca at 400 MeV/u with the Plastic Ball/Wall acceptance and a central trigger simulated. The diagonal straight line indicates where fully thermalized events are expected. In a) the spectator matter is rejected, while it is included in b).

assumed local thermal equilibrium. A crucial question is that of the mean free path of nucleons in these regions of high particle densities. Thermalization in the reaction is characterized by the effect that the originally longitudinal energy is randomized over longitudinal and transverse degrees of freedom. The degree of thermalization can be expressed by the ratio $2 \cdot \sum_{i=1}^{N} |p_\perp|_i \Big/ \pi \cdot \sum_{i=1}^{N} |p_\parallel|_i$. This ratio is shown in fig. 18 as a function of multiplicity for the reaction of 400 MeV/u $^{40}Ca$ on Ca. The ratio is increasing with multiplicity but at least at this energy and target-projectile combination never reaches the value 1, which would be a necessary criterion for thermalization. Cascade calculations with the code of Yariv and Fraenkel[27]), however, show that even a few spectator fragments deform a spherical event in momentum space into a prolate spheroid (fig. 19). From that it is obvious that it is necessary to find a reliable method that is able to distinguish between participants and spectator matter.

## 9.3 GLOBAL ANALYSIS

The global analysis methods (sphericity, thrust) were developed as a tool to detect and distinguish predicted two jet events at high energy $e^+e^-$ storage rings from events with spherically symmetric emission patterns[28]). Both methods define a jet axis, the sphericity by minimizing $\sum_i p_{i\perp}^2$ and the thrust by maximizing $\sum |p_{i\parallel}|$ relative to this axis. The sphericity is calculated analytically by diagonalizing the sphericity tensor. One obtains the orientation of the sphericity axis, e.g. relative to the beam direction and three eigenvalues which define an ellipsoid that describes the shape of the event. The thrust analysis yields in addition to the orientation only the magnitude of the thrust, a quantitative measure distinguishing between isotropic and back-to-back emission.

The use of global methods to analyze the more complex events from heavy ion collisions was proposed by several authors[29,30]). Sphericity ($p^2$) overweights leading particles and gives two nucleons a different weight from a deuteron with the same energy per nucleon. Corrections for these shortcomings have been proposed[30]), e.g. the flow analysis[31]). Since a global analysis has to be performed for each event, statistical fluctuations due to finite number effects and to limited experimental acceptance and efficiency are expected. Experimental data have to be compared with results from an analysis of theoretically calculated events, which have been filtered for experimental acceptance and efficiency. Most theoretical models have not yet reached the sophistication of the experimental equipment in the sense that they are not able to calculate all the measured quantities. Cascade codes do not include composite particles and hydrodynamical codes do not produce event-to-event fluctuations. This makes the comparison between experiment and theory difficult. Complete events generated with a statistical model calculation by Randrup and Fai[32]) will be extremely useful to study the effect of finite number fluctuations and experimental biases. As global analysis allows to determine the shape of the event in phase spaces and takes into account all the measured correlations, it should be well suited to distinguish between emission patterns as predicted by the hydrodynamical and the cascade model. Figure 20 shows the reslt of a flow analysis of 400 MeV/u Ca on Ca data. The angle of the main axis of the flow ellipsoid is plotted versus the square of the ratio of the largest to the smallest axis. A comparison of those results with theoretical predictions can be only done after the calculated events have been filtered for the experimental acceptance. This procedure is presently being developed for cascade events.

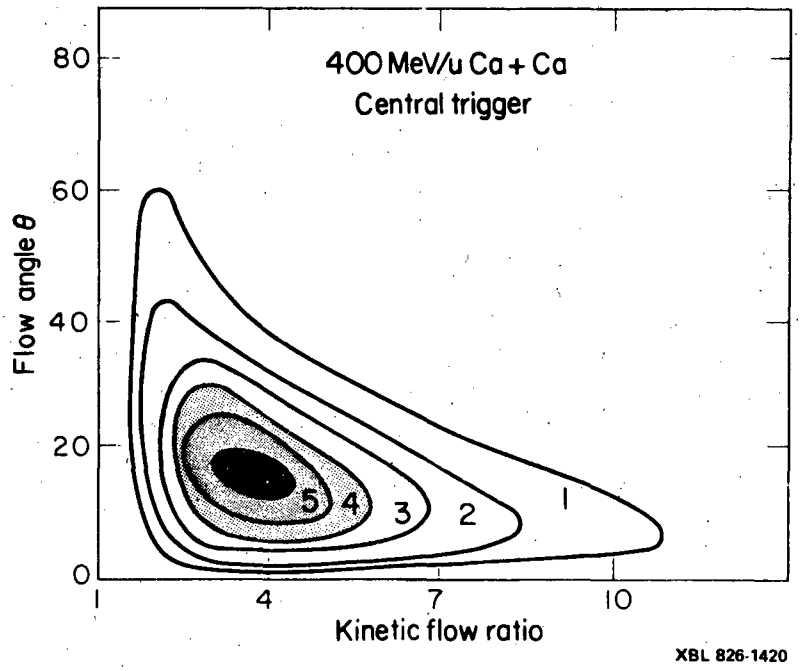


Fig. 20. Flow plot for 400 Mev/u Ca on Ca.

## 10. Conclusions

Through the available $4\pi$ detector data we have shown that the deuteron to proton ratio increases with increasing charge particle multiplicity. This can be explained by phase space considerations taking both the size of the participant volume and the finite size of the deuteron cluster into account. These findings should explain the target-projectile mass dependence of d/p values but shed serious doubts on entropy discussions based on single particle inclusive data which average over impact parameter. From observables such as the ratio of transverse to longitudinal momentum the degree of thermalization can be measured. If equilibrium is found, the concept of temperature can be applied and compared to predictions of various models. Temperature, together with a better understanding of the entropy values, could lead to a big step forward towards the establishment of the equation of state of nuclear matter.

This work was supported in part by the Director, Office of Energy Research, Division of Nuclear Physics of the Office of High Energy and Nuclear Physics of the U.S. Department of Energy under Contract DE-AC03-76SF00098.

## References


1) A. Sandoval, H.H. Gutbrod, W.G. Meyer, A.M. Poskanzer, R. Stock, J. Gosset, J.-C. Jourdain, C.H. King, G. King, Ch. Lukner, Nguyen Van Sen, G.D. Westfall, and K.L. Wolf, Phys. Rev. C21 (1980) 1321.
W.G. Meyer, H.H. Gutbrod, Ch. Lukner, A. Sandoval, Phys. Rev. C22 (1980) 179.
A.I. Warwick, A. Baden, H.H. Gutbrod, M.R. Maier, H.G. Ritter, H. Stelzer, F. Weik, H.H. Wieman, S.B. Kaufman, B.D. Wilkins, E.P. Steinberg, J. Peter, LBL-13831, to be published.
2) J.C. Tompkins, SLAC Report No. 224 and SLAC Report No. 578 (1980) unpublished
E.D. Blum, Proceed. of the 9th International Symposium on Lepton and Photon Interactions at High Energies, Batavia, 1979, edited by T. Kirk and H. Abarbanel, Fermilab, 1980
M. Oreglia, Ph.D. thesis, SLAC Report No. 236 (1980), unpublished
3) D.H. Wilkinson, Rev. of Scient. Inst. 23 (1952) 414
D. Bodansky and S.F. Eccles, Rev. of Scient. Inst. 28 (1957) 464
4) M. Mayhugh of Harshaw Chem. Co., Solon, Ohio, proposed the use of $CaF_2(Eu)$
5) C.I. Industries, Tokorozawa, Japan, plastic scintillator similar to NE114.
6) PM 2202 AMPEREX
7) Crofon 1410 (Dupont) light fiber
8) J. Peter, LBL internal report 1979, unpublished
9) R. Maday and W. Schimmerling, private communications
10) Silicon PIN photo diode, SGD-100A, EG&G Electro optics, 35 Congress St., Salem, MA 10970
11) H.H. Gutbrod, M.E. Maier, H.G. Ritter, A.I. Warwick, F. Weik, H. Wieman, and K.L. Wolf, IEEE Transactions on Nuclear Science, Vol. NS-28, No. 1, February 1981
12) P. Siemens and J. Kapusta, Phys. Rev. Lett. 43 (1979) 1486
13) H. Stöcker, LBL-12302 (April 1981)
14) J. Knoll, L. Münchow, G. Röpke, and J. Schulz, Phys. Lett. 112B (1982) 13
15) G. Bertsch and J. Cugnon, Phys. Rev. C24 (1981) 2514; and J. Cugnon, Proc. of ICOSAHIR, Nucl. Phys. A387 (1982) 191c
16) S. DasGupta, B.R. Jennings, and J.I. Kapusta, Phys. Rev. C26 (1982) 274
17) T. Biró, H.W. Barz, B. Lukács, and F. Zimányi, to be published
18) R.K. Tripathi, Phys. Rev. C25 (1982) 1114
19) H.H. Gutbrod, A. Sandoval, P.J. Johansen, A.M. Poskanzer, J. Gosset, W.G. Meyer, G.D. Westfall, and R. Stock, Phys. Rev. Lett. 37 (1976) 667
20) A.Z. Mekjian, Phys. Rev. C17 (1978) 1051
21) S. Nagamiya, M.C. Lemaire, E. Moeller, S. Schnetzer, G. Shapiro, H. Steiner, and I. Tanihata, Phys. Rev. C24 (1982) 971
22) H.H. Gutbrod, A.I. Warwick, and H. Wieman, Proc. of Maria Workshop, Banff, Canada, and Proc. of ICOSAHIR, Nucl. Phys. A387 (1982) 177c
23) J. Kapusta, Phys. Rev. C21 (1980) 1301
24) B.R. Jennings, S. DasGupta, and N. Mobed, Phys. Rev. C25 (1982) 278
25) H. Sato and K. Yazaki, Phys. Lett. 98B (1981) 153
26) H. Stöcker, W. Greiner, and W. Scheid, Z. Physik A286 (1978) 121
H. Stöcker, J.A. Maruhn, and W. Greiner, Phys. Lett. 81B (1979) 303
27) Y. Yariv and Z. Fraenkel, Phys. Rev. C20 (1979) 2227
28) S. Brandt and H. Dahmen, Z. Physik C1 (1979) 61
29) J. Kapusta and D. Strottman, Phys. Lett. 106B (1981) 33
30) J. Knoll, Proceedings 5th High Energy Heavy Ion Study, LBL-12652 (1981)
31) M. Gyulassy, K.A. Frankel, and H. Stöcker, Phys. Lett. 110B (1982) 185
32) J. Randrup and G. Fai, Phys. Lett. 115B (1982) 281

This report was done with support from the Department of Energy. Any conclusions or opinions expressed in this report represent solely those of the author(s) and not necessarily those of The Regents of the University of California, the Lawrence Berkeley Laboratory or the Department of Energy.

Reference to a company or product name does not imply approval or recommendation of the product by the University of California or the U.S. Department of Energy to the exclusion of others that may be suitable.

*TECHNICAL INFORMATION DEPARTMENT*
*LAWRENCE BERKELEY LABORATORY*
*UNIVERSITY OF CALIFORNIA*
*BERKELEY, CALIFORNIA 94720*